46th AIAA/ASME/SAE/ASEE Joint Propulsion Conference & Exhibit
25 - 28 July 2010, Nashville, TN

AIAA 2010-6844

Modeling Mach Number and Temperature Distributions in Supersonic Nozzle Flow

Joseph Majdalani* and Brian A. Maicke†
University of Tennessee Space Institute, Tullahoma, TN 37388

Stodola's area-Mach number relation is one of the most widely used expressions in compressible flow analysis. From academe to aero-propulsion, it has found utility in the design and performance characterization of numerous propulsion systems; these include rockets, gas turbines, micro-combustors, and micro-thrusters. In this study, we derive a closed form approximation for the inverted and more commonly used solution relating performance directly to the nozzle area ratio. The inverted expression provides a computationally efficient alternative to solutions based on traditional lookup tables and root finding. Here both subsonic and supersonic Mach numbers are obtained explicitly as a function of the area ratio and the ratio of specific heats. The corresponding recursive formulations enable us to specify the desired solution to any level of precision. In closing, a dual verification is achieved using a CFD simulation of a typical nozzle and through Bosley's formal approach intended to confirm the truncation error entailed in our approximations. In this process, both asymptotic and numerical solutions are compared for the Mach number and temperature distributions throughout the nozzle.

Nomenclature

A	=	local cross sectional area
A_t	=	nozzle throat area
E_n	=	absolute error between M_N and M_n
M_n	=	asymptotic property at iteration order n
M_N	=	numeric property reflecting true value
ε	=	perturbation parameter, A_t / A
γ	=	ratio of specific heats

Subscripts and Symbols

0 , 1	=	leading and first order
c	=	condition in the combustion chamber
e	=	condition in the exit plane
n	=	asymptotic level
N	=	numerically calculated value
t	=	condition at the nozzle throat
$\underline{\ }$	=	subsonic term

I. Introduction

THE design of a supersonic nozzle may be viewed as an optimization study in which the exit Mach number plays the role of a target variable defined by mission requirements. In this vein, a wide variability exists as virtually any smooth curve can be used in the subsonic region so long as the concavity of the contracting section does not prompt flow separation. In the throat section, curvature is minimized to promote the establishment of a uniform

*H. H. Arnold Chair of Excellence in Advanced Propulsion, Mechanical, Aerospace and Biomedical Engineering Department. Senior Member AIAA. Fellow ASME.
†Graduate Research Assistant, Mechanical, Aerospace and Biomedical Engineering Department. Member AIAA.

choking plane. Downstream of the throat, the flow is accelerated to supersonic levels across an expanding section. In this region, proper contouring becomes critically important as discontinuities in the Prandtl-Meyer angle can cause undesirable shocks and expansions. In the vicinity of the exit plane, the curvature is re-straightened to reduce flow divergence losses. While traditional techniques, such as the method of characteristics, can be employed to arrive at an optimal nozzle shape, computational fluid dynamics (CFD) can also be used as a modern alternative.

In addition to the geometric optimization challenges, thermal protection issues arise in practical nozzle manufacture. These are often associated with the temperature distribution and heat fluxes resulting at the walls. On the one hand, enhancing performance and payload capability entails reducing weight and tapering edges. On the other hand, thermal protection against exhaust gases requires strong materials and optimally designed cross sections. To gradually straighten the flow out of the nozzle, a relatively long, slowly sloping skirt is required to the extent that choosing a suitable length becomes an optimization process in its own right, specifically, one that gauges weight constraints, geometry, and divergence losses. It can thus be seen that the initial design phase of a nozzle relies on an iterative process in which a multitude of calculations are required and where isentropic tools can be readily employed due to their ease and relative accuracy.

During this iterative process, several isentropic flow approximations in converging-diverging nozzles may be used and these are based on the area-Mach number relation connecting the Mach number to the nozzle area ratio and gas properties. Since its inception in 1903 by Stodola,[1] this key expression has led to a substantial leap in our understanding of supersonic nozzle behavior;[2,3] today, it can be found in most fundamental textbooks on the subject.[3-7]

Stodola's relation has been verified both experimentally[1] and more recently via CFD.[8,9] It is used in compressible flow simulations of the internal flowfield in solid rocket motors by Cheng, Liu and Sirignano,[10] Jackson, Najjar and Buckmaster,[11] and Stewart *et al.*[12] It appears in one segment of Rocflu, a compressible Navier-Stokes solver intended for simulating rocket internal ballistics.[11-14] It is also used in characterizing turbomachinery,[15-17] scarfed and contoured-plug nozzles,[18,19] pulse detonation engines,[20,21] and magnetohydrodynamic systems.[22] More recently, it has been employed in applications of constructal theory by Bejan,[23] and in modeling micro-thrusters and micro-combustors by Leach[24] and Tosin *et al.*[25] Its popularity as a simple design tool lies in its ability to predict the area ratio needed to produce a desired exit flow Mach number. This feature is, however, not analytically invertible due to the transcendental nature of the Mach number dependence. At present, one must resort to tabulation or root finding in the process of estimating the expected exit Mach number for fixed area ratio and specific gas properties. In this study, we overcome this difficulty through the use of asymptotics.

The inversion of a Mach number relation via asymptotics is not a novel concept. In similar context, the Prandtl-Meyer function has been treated by a number of researchers such as Probstein[26] who introduced an analytical inversion of the Prandtl-Meyer function for particular values of the specific heat ratio. Day[27] is also known for developing a hybrid inversion using a mix of analytical and computational tools. While these methods vary from those employed here, they lend support to the usefulness of analytical approximations for problems that arise in similar physical contexts. The present relation will be derived with a sufficient degree of accuracy to serve as a direct and practical design alternative. Not only will this solution increase our repertoire of known approximations for compressible flow models, but it will also provide a simple alternative to tabulation and root finding.

II. Formulation

For isentropic flow through a converging-diverging nozzle with throat area A_t, a transcendental equation relates the area ratio, $\varepsilon = A_t / A$, and the local Mach number M at any cross section of surface area A. We are particularly interested in the so-called nozzle expansion ratio for which A corresponds to the maximum area A_e in the nozzle exit plane. From an asymptotic perspective, this condition results in the smallest possible $\varepsilon = \varepsilon_e$. In order to calculate the exit Mach number for a given nozzle design ratio, one can solve for M using a numerical root finding technique appropriate for

$$\varepsilon\left[1+\tfrac{1}{2}(\gamma-1)M^2\right]^{\frac{(\gamma+1)}{2(\gamma-1)}} - M\left[1+\tfrac{1}{2}(\gamma-1)\right]^{\frac{(\gamma+1)}{2(\gamma-1)}} = 0 \tag{1}$$

In general, γ varies between 1.1 and 1.67. In rocket motors, γ varies between 1.1 and 1.4 with an average value of 1.25. For example, the Reusable Solid Rocket Motor (RSRM) has an average molecular weight $M_w = 28.46$ kg/kmol, constant specific heats $C_p = 1966.54$ J/kg-K and $C_v = 1674.4$ J/kg-K, a specific gas constant $R = 292.14$ J/kg-K, a mean chamber pressure $p_0 = 6.28$ MPa, a ratio of specific heats $\gamma = 1.17$, and an

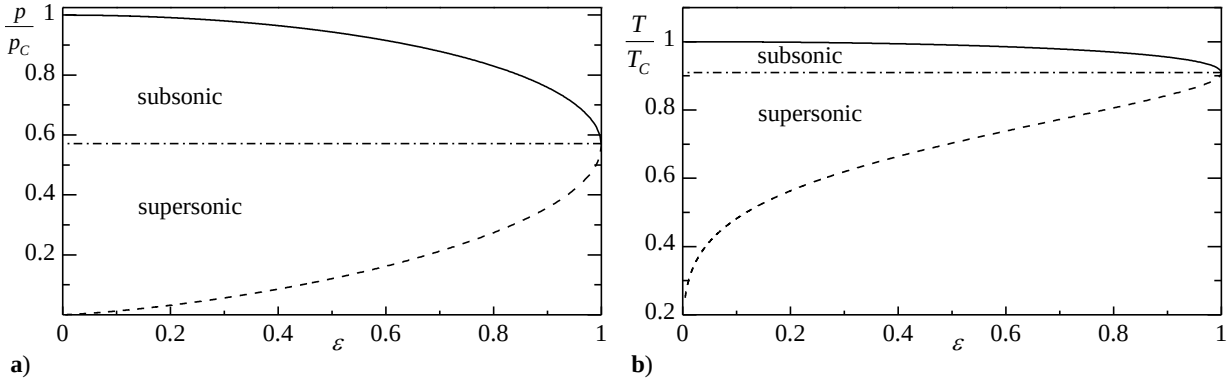

Figure 1. Sensitivity of the pressures and temperatures to the nozzle expansion ratio at $\gamma = 1.4$.

exit area ratio $\varepsilon_e = 0.13$. The exit Mach number is typically larger than 2 and can, of course, be calculated from Eq. (1). According to Sutton,[7] the exit value can range from as low as 2.5 to as high as 10, with most being in a 4-6 range. What is important is that, in many applications, the area ratio ε_e varies between $1/3$ and $1/25$.[7] For high altitude applications (100 km or higher), ε_e ranges between $1/400$ and $1/40$; here the exit areas are increased to accommodate expansions to lower external pressures. To be conservative, one may then assume

$$0.002 \le \varepsilon_e \le 0.4 \tag{2}$$

The natural emergence of a small quantity ε is the motivation for using perturbation methods. These permit the construction of asymptotic solutions for the area-Mach number $M = \mathrm{M}(\varepsilon, \gamma)$ that encapsulate both roots of Eq. (1).

Once the Mach number is determined it can be used to predict the spatial evolution of the temperature, pressure, and density throughout the nozzle. Because Stodola's equation remains an idealized case, it may be used in conjunction with isentropic relations such as,

$$T = T_c / \left[1 + \tfrac{1}{2}(\gamma - 1) M^2\right], \qquad p = p_c / \left[1 + \tfrac{1}{2}(\gamma - 1) M^2\right]^{\frac{\gamma}{\gamma - 1}}, \qquad \rho = \rho_c / \left[1 + \tfrac{1}{2}(\gamma - 1) M^2\right]^{\frac{1}{\gamma - 1}} \tag{3}$$

where p_c, T_c, and ρ_c stand for stagnation chamber properties. Clearly, substitution of $M = \mathrm{M}(\varepsilon, \gamma)$ in the above will give rise, by direct extension, to $T = \mathrm{T}(\varepsilon, \gamma, T_c)$, $p = \mathrm{P}(\varepsilon, \gamma, p_c)$, and $\rho = \Theta(\varepsilon, \gamma, \rho_c)$.

The pressure and temperature are of chief interest because the pressure determines, in part, how the nozzle performs for a given geometry, and the construction of the nozzle is dependent, in part, on the wall temperature distribution and its induced thermal gradients. To illustrate these effects, Fig. 1 is used to describe the pressure and temperature distributions in an isentropic nozzle. In this graph, the subsonic pressures and temperatures are seen to exhibit qualitatively similar shapes, starting at a maximum value and decreasing as the flow enters the converging section of the nozzle. The temperature decreases rather gradually as the acceleration in the subsonic region builds progressively. After the flow crosses the throat at $\varepsilon = 1$, the pressures and temperatures continue to decrease. In the case of the pressure, the supersonic branch appears to mirror its subsonic counterpart, with the slight asymmetry being caused by the location of the critical pressure at the throat, here shown for $\gamma = 1.4$. The temperature, however, experiences visibly dissimilar trends. As the flow enters the supersonic region, the temperature steadily decreases, for $\varepsilon \approx 1$, and then drops precipitously as the area ratio approaches zero. This behavior can be attributed to the thermal-to-kinetic energy conversion and its sensitivity to the degree of area expansion. For small values of ε, the substantial gain in Mach number is seen to translate into appreciable temperature differentials, specifically in the nozzle exit section.

III. Analysis

For a fixed area ratio, two Mach numbers are possible depending on whether the axial position is located upstream or downstream of the throat section. In what follows, the asymptotic analysis leading to each of these roots is described.

A. Subsonic Solution

Using ε as our perturbation parameter, an explicit series approximation for the subsonic Mach number, $\bar{M} = \bar{\mathrm{M}}(\varepsilon, \gamma)$, can be pursued. The subsonic series approximation can be obtained using regular perturbations. To

begin, Eq. (1) can be written in subsonic notation. In the interest of clarity, it is helpful to define two constants and a variable,

$$\alpha \equiv \tfrac{1}{2}(\gamma+1)/(\gamma-1);\ \zeta \equiv \left[\tfrac{1}{2}(\gamma+1)\right]^{\alpha};\ \ \tau\left(\bar{M}\right) \equiv \tfrac{1}{2}(\gamma-1)\bar{M}^2 \tag{4}$$

These transform Eq. (1) into

$$\bar{M} = \tfrac{1}{\zeta}\varepsilon\left[1+\tau\left(\bar{M}\right)\right]^{\alpha} \tag{5}$$

Equation (5) represents the reduced relation that needs to be solved for $\bar{M}$. First, one may express $\bar{M}$ in a series of diminishing terms, specifically

$$\bar{M} = x_0 + \varepsilon x_1 + \varepsilon^2 x_2 + \varepsilon^3 x_3 + \varepsilon^4 x_4 + \varepsilon^5 x_5 + \varepsilon^6 x_6 + \mathcal{O}(\varepsilon^7) \tag{6}$$

Second, by inserting Eq. (6) into Eq. (5), one may expand and segregate terms of the same order. At the outset, one finds that terms of even order must strictly vanish:

$$x_0 = x_2 = x_4 = x_6 = 0 \tag{7}$$

In theory, the expansion of $\bar{M}$ will be accurate to $\mathcal{O}(\varepsilon^7)$ when the first three nonzero corrections are retained. The effective expansion reduces to

$$\bar{M} = \varepsilon x_1 + \varepsilon^3 x_3 + \varepsilon^5 x_5 + \mathcal{O}(\varepsilon^7) \tag{8}$$

Subsequently, one may substitute Eq. (8) into Eq. (4) to retrieve a series expression for τ,

$$\tau = \tfrac{1}{2}\varepsilon^2\gamma x_1^{\,2} - \tfrac{1}{2}\varepsilon^2 x_1^{\,2} - \varepsilon^4 x_1 x_3 + \varepsilon^4\gamma x_1 x_3 + \mathcal{O}(\varepsilon^6) \tag{9}$$

One may also use the binomial expansion of Eq. (5) to evaluate

$$\left(1+\tau\right)^{\alpha} = 1 + \alpha\tau + \tfrac{1}{2!}\alpha(\alpha-1)\tau^2 + \tfrac{1}{3!}\alpha(\alpha-1)(\alpha-2)\tau^3 + \ldots \tag{10}$$

and so

$$\zeta^{-1}\varepsilon\left(1+\tau\right)^{\alpha} = \tfrac{1}{\zeta}\varepsilon + \tfrac{1}{\zeta}\varepsilon\alpha\tau + \tfrac{1}{2!\zeta}\varepsilon\alpha(\alpha-1)\tau^2 + \tfrac{1}{3!\zeta}\varepsilon\alpha(\alpha-1)(\alpha-2)\tau^3 + \ldots \tag{11}$$

The binomial expansion in Eq. (11) will be valid for $|\tau| = \tfrac{1}{2}(\gamma-1)\bar{M}^2 < 1$, an expression that remains true in the subsonic case. This is especially true when considering that the ratio of specific heats varies between 1.1 and 1.4 in most propulsive applications. This ensures that $|\tau| \ll 1$ which, in turn, prompts the swift convergence of the series. The left-hand side of Eq. (5) can now be replaced by the perturbed form of $\bar{M}$ such that

$$\zeta^{-1}\left(1+\tau\right)^{\alpha} = \varepsilon x_1 + \varepsilon^3 x_3 + \varepsilon^5 x_5 + \mathcal{O}(\varepsilon^7) \tag{12}$$

The final step is to insert Eq. (11) into Eq. (12). Collecting terms of the same order yields

$$x_1 = \left[\tfrac{1}{2}\left(\gamma+1\right)\right]^{-\alpha},\ \ x_3 = \tfrac{1}{4}\left(\gamma+1\right)x_1^3,\ \ x_5 = \tfrac{1}{32}(\gamma+1)(3\gamma+7)x_1^5 \tag{13}$$

The corresponding Mach number may be obtained to arbitrary order from

$$\bar{M}_n = \sum_{i=0}^{n} \varepsilon^{2i+1} \frac{(2i)!}{i!2^i} \frac{(\gamma-1)^i}{(2i+1)!\zeta^{2i+1}} \prod_{j=0}^{i-1}\left[(2i+1)\alpha - j\right] + \mathcal{O}(\varepsilon^{2n+3}) \tag{14}$$

By way of example, a three-term subsonic series approximation becomes

$$\bar{M}_2 = \varepsilon x_1 + \varepsilon^3 \tfrac{1}{4}\left(\gamma+1\right)x_1^3 + \varepsilon^5 \tfrac{1}{32}(\gamma+1)(3\gamma+7)x_1^5 + \mathcal{O}(\varepsilon^7) \tag{15}$$

It may be later shown that this expression is virtually indiscernible from the numerical solution of the problem. In fact, for operational area ratios up to $\varepsilon = 0.47$ and $\gamma = 1.7$, only one term needs to be calculated and still secure a practical approximation that accrues a less than 5% error. Table 1 catalogues the maximum value of ε for which the error will remain bracketed under 5% at different values of γ and the first three asymptotic orders. Note that the range of validity broadens when more terms are retained or when γ is lowered. The range extends to $\varepsilon = 0.50$ for the lowest value reported, $\gamma = 1.1$. Using a two-term correction, the maximum operational range increases to $0.64 \le \varepsilon \le 0.79$ for $1.1 \le \gamma \le 1.7$, with the largest ε corresponding to the smallest γ. From an engineering perspective, Eq. (15) mirrors the exact solution because

Table 1. Maximum nozzle area ratio with less than 5% relative error at increasing asymptotic orders

	Subsonic			Supersonic		
γ \ n	0	1	2	0	1	2
1.1	0.495	0.794	0.889	n/a	0.948	0.987
1.2	0.491	0.670	0.885	n/a	0.767	0.999
1.3	0.486	0.664	0.883	n/a	0.729	0.962
1.4	0.482	0.658	0.881	0.00631	0.746	0.940
1.5	0.478	0.653	0.879	0.01890	0.773	0.931
1.7	0.470	0.644	0.875	0.06470	0.820	0.930

its error remains smaller than that associated with the governing equation itself; the latter is attendant on the isentropic flow idealization. Hence, by virtue of the physical range defined in Eq. (2), a one-term approximation is sufficient to provide an accurate approximation up to $\varepsilon = 0.40, \ \forall \gamma$. This key result is:

$$\bar{M} \simeq \varepsilon \left[\tfrac{1}{2}(\gamma+1) \right]^{\frac{(\gamma+1)}{2(\gamma-1)}} + \mathcal{O}(\varepsilon^3) \tag{16}$$

Note that ε is not limited to the nozzle expansion ratio. It may correspond to any cross section so long as the inverted ratio with the throat area remains small.

B. Supersonic Solution

Using the method of successive approximations, an explicit series expansion for $M = \mathrm{M}(\varepsilon, \gamma)$ may be obtained. Successive approximations may be applied to polynomials and transcendental relations in which roots are not deducible from a regular expansion, namely, from a predetermined sequence of gauge functions.[28] The ensuing linearization may be achieved by striking a balance in Stodola's equation between terms that dominate for $M > 1$. To this end, we rewrite Eq. (1) in supersonic notation by introducing the three constants β, κ, and μ:

$$\beta \equiv (\gamma+1)/(\gamma-1) \ ; \ \kappa \equiv \sqrt{\tfrac{1}{2}(\gamma-1)} \ ; \ \mu \equiv \varepsilon^{1/\beta} / \sqrt{1+\kappa^2} \tag{17}$$

These may be substituted into Eq. (1) to render the simple form

$$\mu^2 \left(1 + \kappa^2 M^2\right) = M^{2/\beta} \tag{18}$$

Next, M must be expanded carefully. In identifying the leading order part of Eq. (18), we substitute $M_0 = X_0$ into Eq. (18) and write

$$X_0^{2/\beta} - \mu^2 \kappa^2 X_0{}^2 - \mu^2 = 0 \tag{19}$$

A scaling analysis reveals that the first two members of Eq. (19) dominate with the third member representing a secondary contribution. This behavior can be confirmed through the use of a numerically calculated root. For the supersonic case at $\varepsilon \simeq 0.1$, the Mach number is $\mathcal{O}(1)$. When substituting the ordered quantities back into Eq. (19), the first member will be seen to carry the largest contribution. Along similar lines, the second member will exhibit a non-negligible, albeit smaller contribution, owing to its coefficient $\mu^2 = \varepsilon^{2/\beta}$ multiplying its $X_0^2 > 1$ part. The third member in Eq. (19) contains an $\varepsilon^{2/\beta}$ term only; as such, it can be viewed as a higher order quantity. It is important to note that by balancing the first two members, a different leading order equation is achieved. At leading order, the two largest terms will balance when

$$X_0 = \left(\mu\kappa\right)^{\beta/(1-\beta)} + \mathcal{O}[\varepsilon^{\frac{1}{2}(\gamma-1)}] \tag{20}$$

Successive expansions of M may be similarly undertaken by setting $M_1 = X_0 + X_1$. Backward substitution into Eq. (18) leads to a solution for X_1 bearing a truncation error of $\mathcal{O}[\varepsilon^{4(\gamma-1)/(\gamma+1)}]$. For all approximations past X_0, a recurrence relation may be written for X_i in terms of X_{i-1}:

$$\begin{aligned} X_i = \lambda \Big\{ & M_{i-1}\beta\left(M_{i-1}^{2/\beta} - M_{i-1}^2 \beta\kappa^2\mu^2\right) \\ & + M_{i-1}\beta\left[M_{i-1}^{2+2/\beta}\kappa^2\mu^2(\beta^2 - 4\beta + 4) - M_{i-1}^2\beta^2\kappa^2\mu^4 + M_{i-1}^{4/\beta}(2\beta-3) + 2M_{i-1}^{2/\beta}\mu^2(2-\beta)\right]^{1/2} \Big\} \ ; \ i \geq 1 \end{aligned} \tag{21}$$

where

$$\lambda = \frac{1}{2M_{i-1}^{2/\beta}(\beta-2) + M_{i-1}^2\beta^2\kappa^2\mu^2} \tag{22}$$

The higher order solutions may be sequentially obtained from the straightforward sum

$$M_n = X_0 + X_1 + \ldots + X_n \tag{23}$$

Table 1 also lists the area ratios for which the relative error in Eq. (23) will reach 5% at different perturbation orders. To maintain a less than 5% error, a two-term approximation is clearly necessary as the validity of one term expressions is limited. Using $M_1 = X_0 + X_1$, the relevant range of area ratios extends to $[0.73 - 0.95]$ depending on the value of γ. When three terms are held, the valid range is extended to 0.99 at $\gamma = 1.2$. Considering that practical nozzles do not exceed $\varepsilon = 0.4$, a two-term approximation of the form $M \approx M_1$ may be relied on.

Before leaving this section, it may be interesting to note that the γ-dependence differs in behavior between the subsonic and supersonic solutions. In the former, the range of validity in ε improves at lower values of γ. In the latter, more than one local minimum can appear due to the nonlinearity of the supersonic formulation. For $M = M_1$, a local minimum appears in the middle of the feasible range of γ, occurring approximately near $\gamma = 1.3$. The corresponding range of validity in ε subsequently expands as $|\gamma - 1.3|$ is increased.

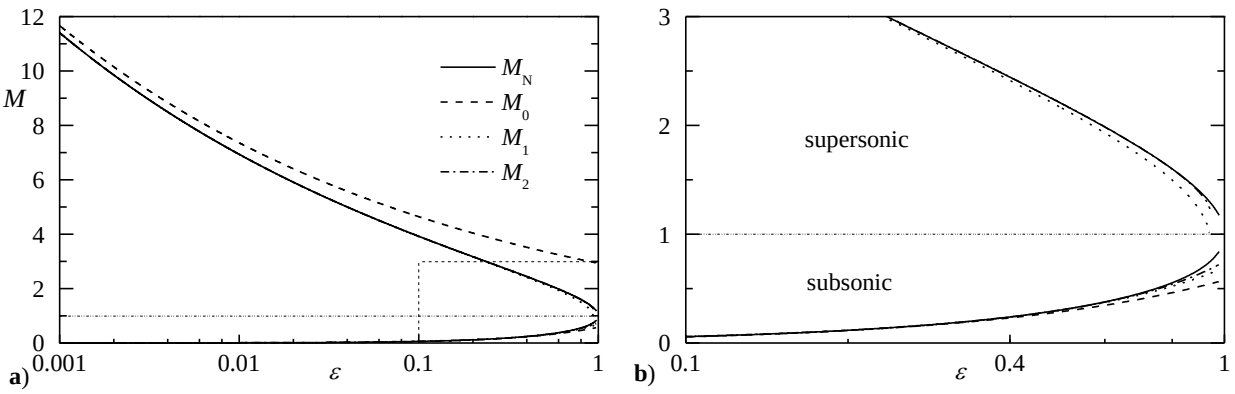

Figure 2. Comparison between numerics and asymptotics in both subsonic and supersonic regimes for γ=1.4.

IV. Comparison and Order Verification

A. Numerical Verification

The approximation for M_n is compared in Fig. 2 to M_N, the numerical solution of Eq. (1), at increasing asymptotic orders, $n = 0,1,2$. Both M_N and M_n are shown in subsonic and supersonic regimes at a representative value of $\gamma = 1.4$. These trends remain unchanged at other γ. The inset in Fig. 2 enhances the differences between numerics and asymptotics in the transonic region. In the meaningful range of $\varepsilon \le 0.4$, the visible discrepancies become indiscernible when using either the one-term subsonic or the two-term supersonic approximations. This behavior concurs with the relative error predictions (reflecting a less than 5% deviation) furnished in Table 1 for $\bar{M}_0$ and M_1. In the vicinity of $\varepsilon = 1$, the discrepancies do not pose a concern as they only denote impractically small nozzle divergences.

B. CFD Verification

An inviscid, axisymmetric, density-based, double precision, finite volume solver is employed to simulate the motion of an ideal gas in a fully-flowing supersonic nozzle. The nozzle has inlet and outlet area ratios of 2.42 and 5.44, respectively. Given an overall nozzle length of L = 0.3 m, the computational domain is resolved using a mesh comprised of 26,801 quadrilateral cells, as shown in Fig. 3. The nozzle contour consists of a simple three-point spline. Using air as the working fluid, two separate validation runs are undertaken. The first trial uses a low pressure, low temperature flow with $T_c = 300\,\text{K}$, while the second simulates a higher chamber pressure and a temperature of $T_c = 2,200\,\text{K}$. The thermodynamic properties specific to each trial are posted in Table 2.

Figure 4 describes the evolution of the velocity vectors and corresponding Mach numbers for the low temperature trial. The velocity scatter and Mach number contours characterize the flow magnification through the converging-diverging nozzle (Figs. 4a-b). Downstream of the throat section, in the supersonic acceleration stage, the particles at the wall outrun the centerline particles. This can be attributed to the absence of friction at the wall and the enhanced radial and axial expansions near the wall due to nozzle divergence; these exceed the centerline expansion that is limited to axial acceleration alone. Being expanded both axially and radially, the flow near the wall experiences increased values of the local Mach number. Conversely, the axially dominated centerline motion undergoes no radial acceleration and, as such, remains limited to a relatively smaller increase in its local Mach number.

The wall, centerline, and average Mach numbers obtained at different stations in the nozzle are compared in Fig. 4c to the three-term analytical approximations. This comparison is carried out point-by-point and shows that the 1-D analytical model lies between the wall and centerline curves, thus providing excellent agreement with the average computed Mach number at any given station. This agreement holds everywhere except in the close vicinity of the throat

Table 2. Parameters used in the low and high temperature simulations with air as the working fluid

Parameter	Cold	Hot
Chamber pressure (Pa)	101,325	506,625
Outlet pressure (Pa)	3,740	50,660
Chamber temperature (K)	300	2,200
Ratio of specific heats	1.4	1.4
Exit area ratio (A_t/A_e)	0.184	0.184

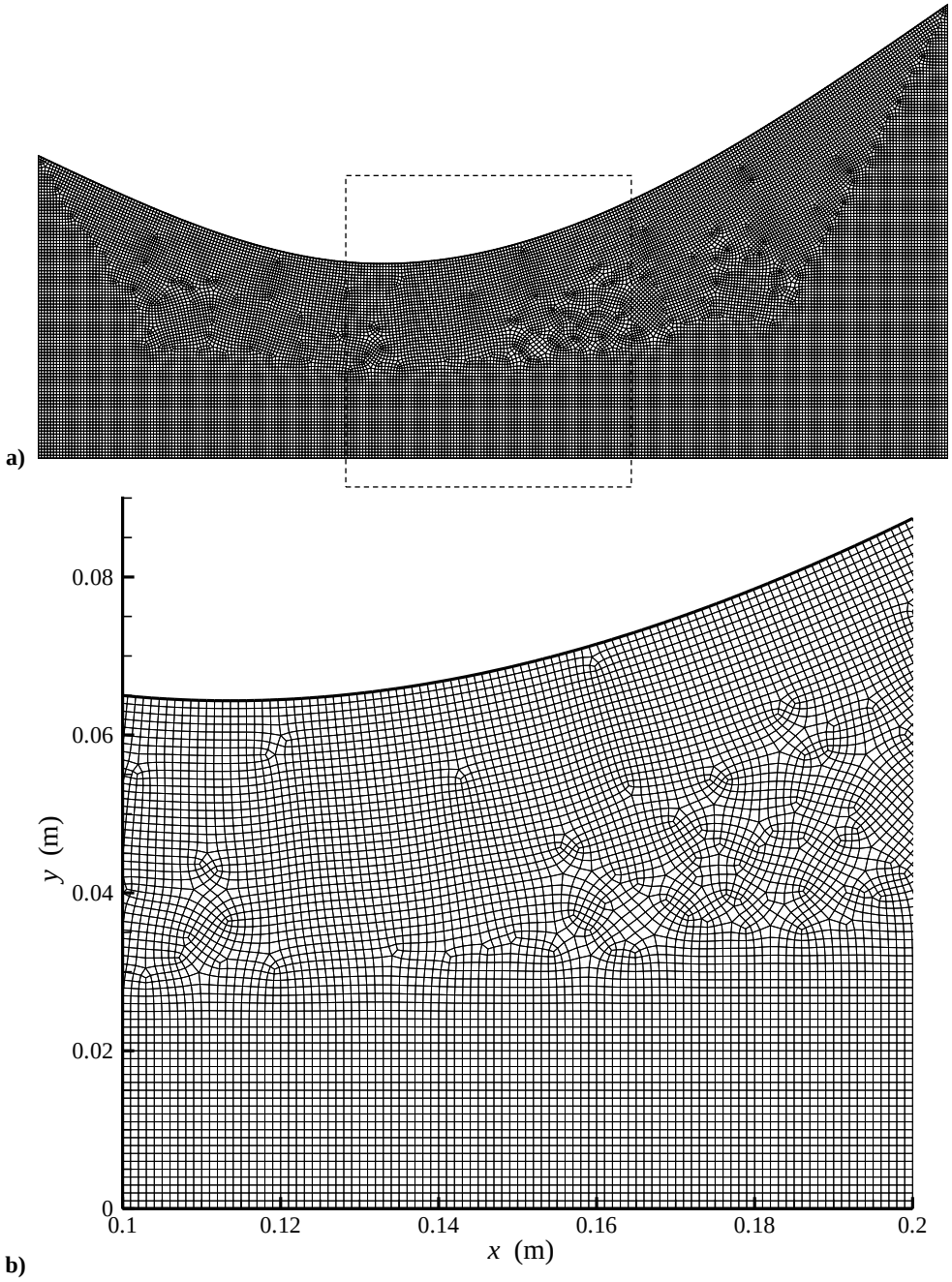

Figure 3. CFD nozzle geometry and mesh selection with enlarged inset.

where the solution begins to diverge as the area ratio approaches unity. This region can be further shrunk by including more corrective terms, although the three-term approximation remains adequate over the vast majority of the nozzle.

Figures 5 and 6 display the thermal data for the low and high chamber temperature runs. As expected, the spatial distribution of the temperature isolines are qualitatively comparable to the Mach number contours, both for the cold (Fig. 5) and hot (Fig. 6) simulations. The temperatures undergo a constant decline as the fluid is accelerated throughout the nozzle, owing to the continual thermal-to-kinetic energy conversion. Figures 5b and 6b compare both trials to the present study using the isentropic relation in Eq. (3). As with the Mach number, the asymptotic approximations are seen to provide an excellent average throughout the nozzle, with small discrepancies being detected in the neighborhood of the throat. The resulting expressions can thus be used as analytical alternatives to

CFD computations in simplified thermal analyses of the nozzle. For example, both Stodola's and CFD solutions predict the occurrence of the maximum heat flux just upstream of the sonic point where the centerline velocity first reaches the speed of sound. This behavior is consistent with experiments[7] and may be seen in Fig. 7 where the normalized heat flux, defined by $q = T/(2\pi r)$, is plotted over the length of the nozzle using Stodola's numerical solution, the present approximation, and CFD predictions. Also shown on the same graph is the spatial variation of the Mach number obtained from Stodola's 1-D model previously described in Fig. 4.

C. Asymptotic Error Verification

To verify the order of the error associated with the subsonic and supersonic perturbation expansions of M, one may apply Bosley's graphical technique.[29] Accordingly, one may confirm that the expansion is asymptotically valid by showing that its absolute error exhibits, in some range of ε, a constant logarithmic rate. For that purpose, the absolute error may be defined as

$$E_n(\varepsilon,\gamma) = \left|M_n - M_{\mathrm{N}}\right|; \bar{E}_n = \left|\bar{M}_n - \bar{M}_{\mathrm{N}}\right| \qquad (24)$$

In either of the subsonic or supersonic cases, if the truncation error appears at order r, one can put

$$E_n(\varepsilon,\gamma) = C\varepsilon^r \qquad (25)$$

Graphically, the order of a given approximation can then be inferred from the log-log plot of E_n versus ε at constant γ. According to Bosley,[29] it is important for the error to approach zero at the correct rate (i.e., $r \to \text{const}$) as $\varepsilon \to 0$.

Forthwith, graphs of $\log E_n$ versus $\log\varepsilon$ are given in Fig. 8 over a practical range of nozzle area ratios and a representative value of $\gamma = 1.4$. Corresponding asymptotic slopes are obtained using linear least-squares and posted in Table 3, including those for $\gamma = 1.2$. It is gratifying to note that all slopes approach constant rates, thus reflecting an 'error-free' analysis.

In the subsonic case, the best fit slopes obtained from least-squares match quite closely the order of the theoretical truncation error given by Eq. (14).

In the supersonic case, the slope begins at a modest rate of descent that can be approximated by $\frac{1}{2}(\gamma-1)$. It then increases rapidly as more terms are added. By retaining two terms, the asymptotic order in M_1 jumps to $4(\gamma-1)/(\gamma+1)$. Being almost quadrupled in comparison to the leading order, M_1 is accompanied by a less than 5% error for practical values of γ and up to $0.73 \le \varepsilon \le 0.95$ (Table 1). In the supersonic case, the order increases with γ. In every case, the slope approaches a constant value with a higher correlation coefficient at higher values of n and in ranges of smaller ε. The slopes shown in Table 3 are evaluated in the $\varepsilon \in [0.001 - 0.01]$ domain. Their agreement with the theoretical orders only improves in ranges of smaller ε.

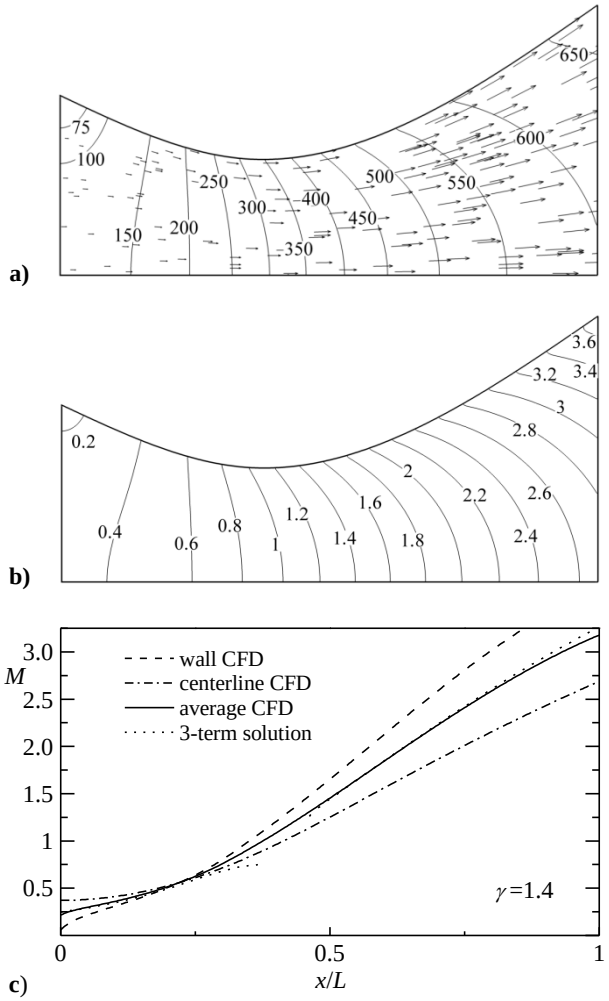

Figure 4. Cold flow simulation results depicting a) velocity vector distribution, b) Mach number contours, and c) comparison of Mach number predictions.

Table 3. Asymptotic slopes in $E_n \sim \varepsilon^r$ using the method of least squares

γ (subsonic)	$\bar{E}_0$	$\bar{E}_1$	$\bar{E}_2$
1.2	3	5	7
1.4	3	5	7
γ (supersonic)	E_0	E_1	E_2
1.2	0.120	0.361	0.929
1.4	0.210	0.635	1.518

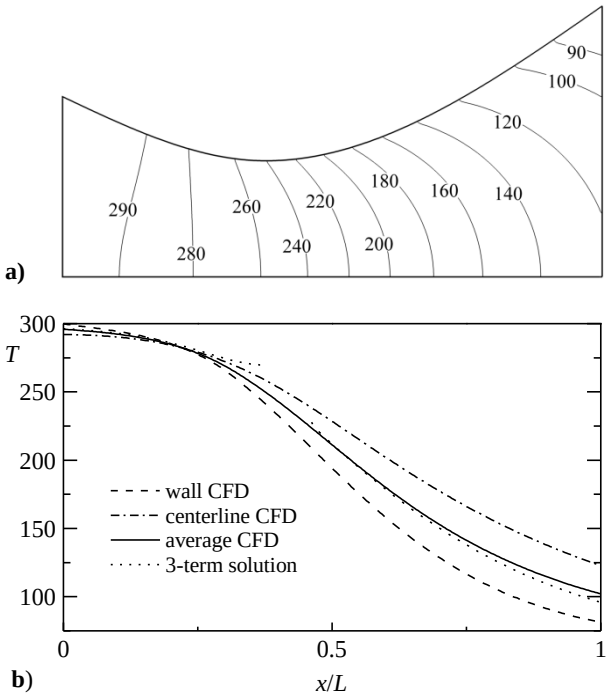

Figure 5. Cold flow results depicting the a) thermal map in K and b) a comparison of wall temperature predictions.

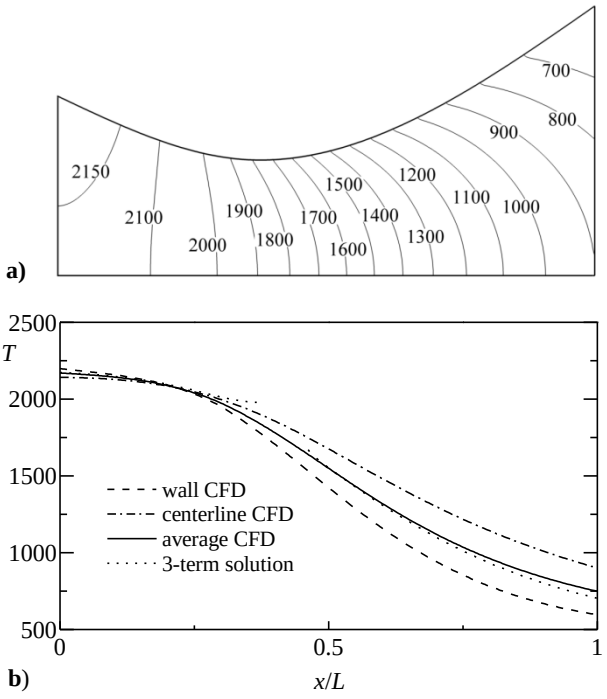

Figure 6. Hot flow results depicting the a) thermal map in K and b) a comparison of wall temperature predictions.

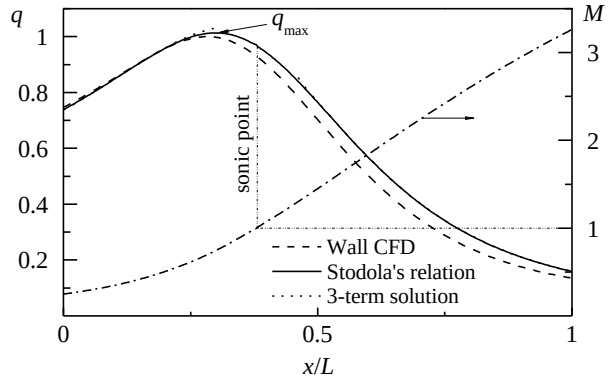

Figure 7. Comparison of normalized heat flux and the spatial evolution of the Mach number.

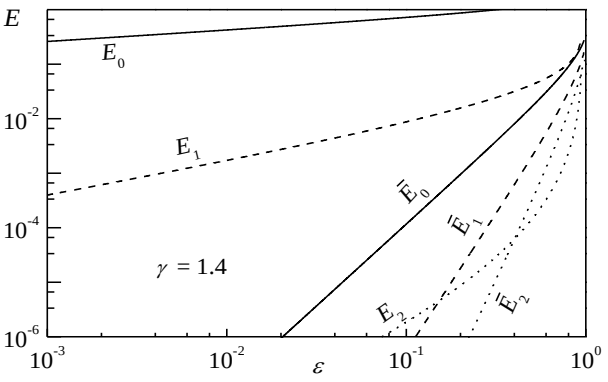

Figure 8. Asymptotic error entailed in supersonic and subsonic solutions for γ=1.4.

V. Conclusions

In this work, two asymptotic approximations are presented as practical equivalents to the numerically-inverted area-Mach number relation. The present analysis provides the explicit dependence of the Mach number on the nozzle area ratio and ratio of specific heats. This dependence illuminates the influence of each of these parameters on the maximum achievable Mach number for isentropic motion. They also facilitate the efficient evaluation of thermodynamic properties while carrying out a performance analysis of a De Laval nozzle. The present results are hoped to be further used in deriving closed-form expressions of other related parameters in compressible flow studies, which often assume inviscid motions. Were viscous effects included in the analysis, they would have resulted in a reduced average velocity, especially near the wall where the flow would be decelerated. If such were the conditions, then Stodola's relation could still provide a good approximation for the Mach number and corresponding temperature distributions near the centerline, where viscous effects are least significant.

Acknowledgments

This project was funded in part by the National Science Foundation under Grant No. CMMI-0928762.

References

[1]Stodola, A., *Steam Turbines*, Springer-Verlag, Berlin, 1903.

[2]Anderson, J. D., "History of High-Speed Flight and Its Technical Development," *AIAA Journal*, Vol. 39, No. 5, 2001, pp. 761-771. doi: 10.2514/2.1385

[3]Anderson, J. D., *Modern Compressible Flow with Historical Perspective*, 3rd ed., McGraw-Hill, New York, 2003.

[4]Fox, R. W., McDonald, A. T., and Pritchard, P. J., *Introduction to Fluid Mechanics*, 6th ed., John Wiley, New York, 2004.

[5]Moran, M. J., and Shapiro, H. N., *Fundamentals of Engineering Thermodynamics*, 5th ed., John Wiley, New York, 2004.

[6]Çengel, Y. A., and Boles, M. A., *Thermodynamics: An Engineering Approach*, 4th ed., McGraw-Hill, New York, 2002.

[7]Sutton, G. P., *Rocket Propulsion Elements*, 6th ed., John Wiley, New York, 1992.

[8]Thakre, P., and Yang, V., "Chemical Erosion of Carbon-Carbon/Graphite Nozzles in Solid-Propellant Rocket Motors," *Journal of Propulsion and Power*, Vol. 24, No. 4, 2008, pp. 822-833. doi: 10.2514/1.34946

[9]Zhang, J., Jackson, T. L., Najjar, F. M., and Buckmaster, J., "High-Fidelity Multiphysics Simulations of Erosion in SRM Nozzles," AIAA Paper 2009-5499, August 2009.

[10]Cheng, F., Liu, F., and Sirignano, W. A., "Nonpremixed Combustion in an Accelerating Transonic Flow Undergoing Transition," *AIAA Journal*, Vol. 45, No. 12, 2007, pp. 2935-2946. doi: 10.2514/1.31146

[11]Jackson, T. L., Najjar, F. M., and Buckmaster, J., "New Aluminum Agglomeration Models and Their Use in Solid-Propellant-Rocket Simulations," *Journal of Propulsion and Power*, Vol. 21, No. 5, 2005, pp. 925-936. doi: 10.2514/1.11888

[12]Stewart, D. S., Tang, K. C., Yoo, S., Brewster, Q., and Kuznetsovy, I. R., "Multiscale Modeling of Solid Rocket Motors: Computational Aerodynamics Methods for Quasi-Steady Burning," *Journal of Propulsion and Power*, Vol. 22, No. 6, 2006, pp. 1382-1388. doi: 10.2514/1.16111

[13]Najjar, F. M., Haselbacher, A., Ferry, J. P., Wasistho, B., Balachandar, S., and Moser, R., "Large-Scale Multiphase Large-Eddy Simulation of Flows in Solid-Rocket Motors," AIAA Paper 2003-3700, June 2003.

[14]Buckmaster, J., Jackson, T. L., Massa, L., Najjar, F. M., and Wang, X., "The Current State of Heterogeneous Propellant Combustion Modeling," AIAA Paper 2005-0360, January 2005.

[15]Cumpsty, N. A., and Greitzer, E. M., "Ideas and Methods of Turbomachinery Aerodynamics: A Historical View " *Journal of Propulsion and Power*, Vol. 20, No. 1, 2004, pp. 15-26. doi: 10.2514/1.9176

[16]Farokhi, S., "Analysis of Rotor Tip Clearance Loss in Axial-Flow Turbines," *Journal of Propulsion and Power*, Vol. 4, No. 5, 1992, pp. 452-457. doi: 10.2514/3.23087

[17]Schobeiri, T., and Abouelkheir, M., "Row-by-Row Off-Design Performance Calculation Method for Turbines," *Journal of Propulsion and Power*, Vol. 8, No. 4, 1992, pp. 823-828. doi: 10.2514/3.23555

[18]Ashby, R. L., and Boraas, S., "Installed Thrust Vector for Scarfed Nozzles," *Journal of Spacecraft and Rockets*, Vol. 6, No. 12, 1969, pp. 1410-1415. doi: 10.2514/3.29839

[19]Dosanjh, D. S., and Das, I. S., "Aeroacoustics of Supersonic Jet Flows from a Contoured Plug-Nozzle," *AIAA Journal*, Vol. 26, No. 8, 1988, pp. 924-931. doi: 10.2514/3.9992

[20]Eidelman, S., Grossmann, W., and Lottati, I., "Review of Propulsion Applications and Numerical Simulations of the Pulsed Detonation Engine Concept," *Journal of Propulsion and Power*, Vol. 7, No. 6, 1991, pp. 857-865. doi: 10.2514/3.23402

[21]Dean, A. J., "Recent Developments in Approaches to Pulsed Detonation Propulsion " AIAA Paper 2003-4510, July 2003.

[22]Camberos, J. A., Moorhouse, D. J., and Suchomel, C. F., "Quantifying Irreversible Losses for Magnetohydrodynamic Flow Analysis and Design Integration," *Journal of Thermophysics and Heat Transfer*, Vol. 19, No. 1, 2005, pp. 87-94. doi: 10.2514/1.5547

[23]Bejan, A., "Constructal Theory: Tree-Shaped Flows and Energy Systems for Aircraft," *Journal of Thermophysics and Heat Transfer*, Vol. 40, No. 1, 2003, pp. 43-48. doi: 10.2514/2.3055

[24]Leach, T. T., "Effect of Structural Heat Conduction on the Performance of Micro-Combustors and Micro-Thrusters," Ph.D. Dissertation, University of Maryland, 2005.

[25]Tosin, M. C., Granziera, F., Gibim, F., and Canola, S. T., "A Solid Propellant Micro Thruster Design – a Brief Discussion About Its Viability and Applications," AIAA Paper 2004-6729, November 2004.

[26]Probstein, R. F., "Inversion of the Prandtl-Meyer Relation for Specific Heat Ratios of 5/3 and 5/4," *Journal of Aeronautical Sciences*, Vol. 24, No. 4, 1957, pp. 316-317.

[27]Day, J. D., "Hybrid Computer Inversion of the Prandtl-Meyer Function," *Transactions of the International Association for Mathematics and Computers in Simulation*, Vol. 18, No. 4, 1976, pp. 201-203. doi: 10.1016/0378-4754(76)90001-X

[28]Murdock, J., *Perturbations: Theory and Methods*, John Wiley, New York, 1991.

[29]Bosley, D. L., "A Technique for the Numerical Verification of Asymptotic Expansions," *SIAM Review*, Vol. 38, No. 1, 1996, pp. 128-135. doi: 10.1137/1038006